



# **JGR Space Physics**

## RESEARCH ARTICLE

10.1029/2023JA031648

## **Key Points:**

- Observations of plasma and field characteristics near the source region of a substorm auroral brightening at L ~ 5
- Pi2, auroral luminosity variation and fluctuations of in-situ electromagnetic field and particle flux were observed during substorm onset
- Correspondence between these fluctuations suggest waves in the magnetosphere like ballooning instability control auroral intensity

#### **Supporting Information:**

Supporting Information may be found in the online version of this article.

#### Correspondence to:

L. Chen, chen.liwei@isee.nagoya-u.ac.jp

#### Citation:

Chen, L., Shiokawa, K., Miyoshi, Y., Oyama, S., Jun, C.-W., Ogawa, Y., et al. (2023). Correspondence of Pi2 pulsations, aurora luminosity, and plasma flux fluctuation near a substorm brightening aurora: Arase observations. *Journal of Geophysical Research: Space Physics*, 128, e2023JA031648. https://doi.org/10.1029/2023JA031648

Received 27 APR 2023 Accepted 22 SEP 2023

#### **Author Contributions:**

Conceptualization: K. Shiokawa
Data curation: K. Shiokawa, Y. Miyoshi,
S. Oyama, C.-W. Jun, Y. Ogawa, K.
Hosokawa, Y. Kazama, S. Y. Wang, S.
W. Y. Tam, T. F. Chang, B. J. Wang, K.
Asamura, S. Kasahara, S. Yokota, T. Hori,
K. Keika, Y. Kasaba, A. Kumamoto,
F. Tsuchiya, M. Shoji, Y. Kasahara, A.
Matsuoka, I. Shinohara, S. Nakamura
Formal analysis: L. Chen
Funding acquisition: K. Shiokawa, Y.

Miyoshi
Investigation: L. Chen
Methodology: K. Shiokawa
Project Administration: K. Shiokawa
Y. Miyoshi, Y. Kazama, K. Asamura,
S. Kasahara, S. Yokota, Y. Kasaba, Y.
Kasahara, A. Matsuoka, I. Shinohara

Correspondence of Pi2 Pulsations, Aurora Luminosity, and Plasma Flux Fluctuation Near a Substorm Brightening Aurora: Arase Observations

L. Chen¹ , K. Shiokawa¹ , Y. Miyoshi¹ , S. Oyama¹,² , C.-W. Jun¹ , Y. Ogawa² , K. Hosokawa³ , Y. Kazama⁴ , S. Y. Wang⁴ , S. W. Y. Tam⁵, T. F. Chang¹,⁵, B. J. Wang⁴, K. Asamura⁶ , S. Kasahara⁻ , S. Yokota⁶ , T. Hori¹ , K. Keika⁻ , Y. Kasabaց , A. Kumamoto⁰ , F. Tsuchiya⁰ , M. Shoji¹ , Y. Kasahara¹⁰ , A. Matsuoka¹¹, I. Shinohara⁶ , and S. Nakamura¹ .

<sup>1</sup>Institute for Space-Earth Environmental Research, Nagoya University, Nagoya, Japan, <sup>2</sup>National Institute of Polar Research, Tokyo, Japan, <sup>3</sup>The University of Electro-Communications, Chofu, Japan, <sup>4</sup>Institute of Astronomy and Astrophysics, Academia Sinica, Taipei, Taiwan, <sup>5</sup>Institute of Space and Plasma Sciences, National Cheng Kung University, Tainan, Taiwan, <sup>6</sup>Institute of Space and Astronautical Science, Japan Aerospace Exploration Agency, Sagamihara, Japan, <sup>7</sup>University of Tokyo, Tokyo, Japan, <sup>8</sup>Osaka University, Toyonaka, Japan, <sup>9</sup>Tohoku University, Sendai, Japan, <sup>10</sup>Kanazawa University, Kanazawa, Japan, <sup>11</sup>Data Analysis Center for Geomagnetism and Space Magnetism, Graduate School of Science, Kyoto University, Kyoto, Japan

**Abstract** Although many substorm-related observations have been made, we still have limited insight into propagation of the plasma and field perturbations in Pi2 frequencies (~7-25 mHz) in association with substorm aurora, particularly from the auroral source region in the inner magnetosphere to the ground. In this study, we present conjugate observations of a substorm brightening aurora using an all-sky camera and an inner-magnetospheric satellite Arase at  $L \sim 5$ . A camera at Gakona (62.39°N, 214.78°E), Alaska, observed a substorm auroral brightening on 28 December 2018, and the footprint of the satellite was located just equatorward of the aurora. Around the timing of the auroral brightening, the satellite observed a series of quasi-periodic variations in the electric and magnetic fields and in the energy flux of electrons and ions. We demonstrate that the diamagnetic variations of thermal pressure and medium-energy ion energy flux in the inner magnetosphere show approximately one-to-one correspondence with the oscillations in luminosity of the substorm brightening aurora and high-latitudinal Pi2 pulsations on the ground. We also found their anti-correlation with low-energy electrons. Cavity-type Pi2 pulsations were observed at mid- and low-latitudinal stations. Based on these observations, we suggest that a wave phenomenon in the substorm auroral source region, like ballooning type instability, play an important role in the development of substorm and related auroral brightening and high-latitude Pi2, and that the variation of the auroral luminosity was directly driven by keV electrons which were modulated by Alfven waves in the inner magnetosphere.

**Plain Language Summary** One of the most frequent disturbances in the Earth's magnetosphere is called substorm. Through Earth's magnetic field line, the development of a magnetospheric substorm is projected onto Earth's high-latitude ionosphere as auroral evolution. During a substorm, the energy in the tail of the magnetosphere is released to the earth, and quite a part of this energy is transmitted as different types of wave phenomena. These wave oscillations can be observed by magnetometers on the ground and satellites in the magnetosphere. It is still uncertain what mechanisms trigger these substorm-related waves, how these waves correlate with other substorm phenomena, and how they transmit and dissipate, especially for the wave phenomena at  $\sim$ 4–7 Earth radii away from the Earth. This paper presents a case study of such substorm event, where we show the variation of magnetic field and auroral luminosity on the ground, and the electromagnetic wave that is called as Pi2 pulsations and oscillation of plasma flux in the inner magnetosphere. We demonstrate that there are one-to-one correspondences in these oscillations. We suggest the possibility that a ballooning plasma instability triggers the observed oscillations in particle flux, as well as the electromagnetic wave that modulates the auroral luminosity.

© 2023. American Geophysical Union. All Rights Reserved.

CHEN ET AL. 1 of 17

Resources: C.-W. Jun, Y. Ogawa, K. Hosokawa, Y. Kazama, S. Y. Wang, S. W. Y. Tam, T. F. Chang, B. J. Wang, K. Asamura, S. Kasahara, S. Yokota, K. Keika, Y. Kasaba, A. Kumamoto, F. Tsuchiya, M. Shoji, Y. Kasahara, A. Matsuoka, I. Shinohara, S. Nakamura Software: L. Chen, K. Shiokawa, C.-W. Jun, T. Hori, S. Nakamura Supervision: K. Shiokawa Validation: L. Chen, C.-W. Jun Visualization: L. Chen Writing - original draft: L. Chen Writing - review & editing: L. Chen. K. Shiokawa, Y. Miyoshi, S. Oyama, Y. Ogawa, T. Hori

#### 1. Introduction

Substorm occurs frequently in Earth's magnetosphere and releases the magnetic energy stored in the magnetotail to the inner magnetosphere and ionosphere. The study of substorms helps us to understand the fundamental transport path of the energy from solar wind to Earth's magnetosphere and ionosphere. It is widely known that before and at a substorm onset, low-frequency pulsations are usually detected by ground magnetometers, which are usually referred to as Pi2 pulsations (Olson, 1999; Saito et al., 1976). The Pi2 pulsation is typically defined as irregular pulsations with periods of 40–150 s lasting for a short duration (~10 min). Using various satellites and ground-based instruments, substorm-related Pi2 have been found to occur in many places in the night-side geospace including plasmasphere, plasmasheet, plasmasheet boundary layer, and lobe, coupled with formation of substorm current wedge (SCW) (e.g., Lester et al., 1984; Uozumi et al., 2020), plasma instability (e.g., Keiling, 2012; Solovyev et al., 2000), bursty bulk flow (BBF) (e.g., Kepko et al., 2001; Keiling et al., 2014; Nishimura et al., 2012) and reconnection (e.g., Keiling et al., 2006; Singer et al., 1988). These observations indicate that Pi2 pulsation is an essential signature of the substorm and related processes, and thus, the study of Pi2 could play a key role to understand the development of magnetospheric disturbances and energy transport at substorm onset.

The aurorae are a projection of magnetospheric plasma dynamics onto the ionosphere. It has been suggested in previous studies that oscillations of the electromagnetic field and plasma flux in the Pi2 frequency (~7–25 mHz) are related to substorm auroral intensification and wave structures. For example, Saka et al. (1999) showed one-to-one correspondences between auroral luminosity variation observed in Antarctica and low-latitudinal Pi2 pulsations. Solovyev et al. (2000) showed that the Pi2 oscillation period at high latitudes correspond to the ratio between the spatial scale of auroral wave-like oscillating structures and the propagation speed of the aurorae, and the hodograms of Pi2 showed that the Pi2 polarization was consistent with directions of the auroral vortex. They conclude that auroral wave-like structures are the result of a plasma instability developing in the magnetosphere. Shiokawa et al. (2002) presented a case study showing that Pi2 packets have good correspondence with auroral poleward expansions, though the auroral luminosity is not correlated with low- and high- latitudinal Pi2 pulsations. Using Time History of Events and Macroscale Interactions during Substorms (THEMIS), LANL-97A, Polar satellites, and various magnetometers, Keiling et al. (2008) made a comprehensive study of a substorm event and showed one-to-one correspondences between high-latitudinal Pi2 pulsations, auroral intensification, and energetic ion injections at ~10 Re, suggesting that ballooning instability, a plasma sheet instability that is triggered by an earthward pressure gradient (Roux et al., 1991), is a possible mechanism to trigger the associated variations in these phenomena. Nishimura et al. (2012) made a multi-events study of substorm onset using all-sky imager (ASIs) and magnetometers and showed that each pulse of Pi2 pulsations are associated with auroral poleward intensification. Despite plenty of Pi2 pulsation studies, however, the correlations between the oscillations in the magnetosphere and on the ground have not been well understood. Few conjugate studies have been reported for Pi2-related substorm aurora using ground auroral imagers and conjugate magnetospheric satellites with a comprehensive measurement of the electromagnetic field and plasma, particularly in the earthward vicinity of the source region of the brightening aurora in the inner magnetosphere, which is key to revealing whether the substorm Pi2 is generated in the plasmasphere, and how Pi2 and its energy propagates toward ionosphere and finally dissipates in the ionosphere.

In this paper we report conjugate observations of a substorm event using the Arase (also named as The Exploration of energization and Radiation in Geospace, ERG) satellite at  $L \sim 5$  and an all-sky camera at Gakona, Alaska. Footprint mapping of the satellite shows that the Arase satellite was located just equatorward of the substorm auroral arc during the auroral brightening. We find possible correspondence between auroral luminosity variations, high-latitudinal Pi2 pulsations, and ion injection and their anti-correlation with low-energy electron energy flux. We also observed cavity-type Pi2 pulsations at mid- and low-latitudinal magnetometers. From these observations, we suggest that auroral luminosity variation is closely related to the Alfven wave and plasma flux oscillations in the inner magnetosphere, where ballooning instability may play a role.

#### 2. Instrumentation

The field and plasma data in the inner magnetosphere used in this study were obtained from the Arase satellite. The Arase satellite was developed by the Institute of Space and Astronautical Science (ISAS), Japan Aerospace

CHEN ET AL. 2 of 17

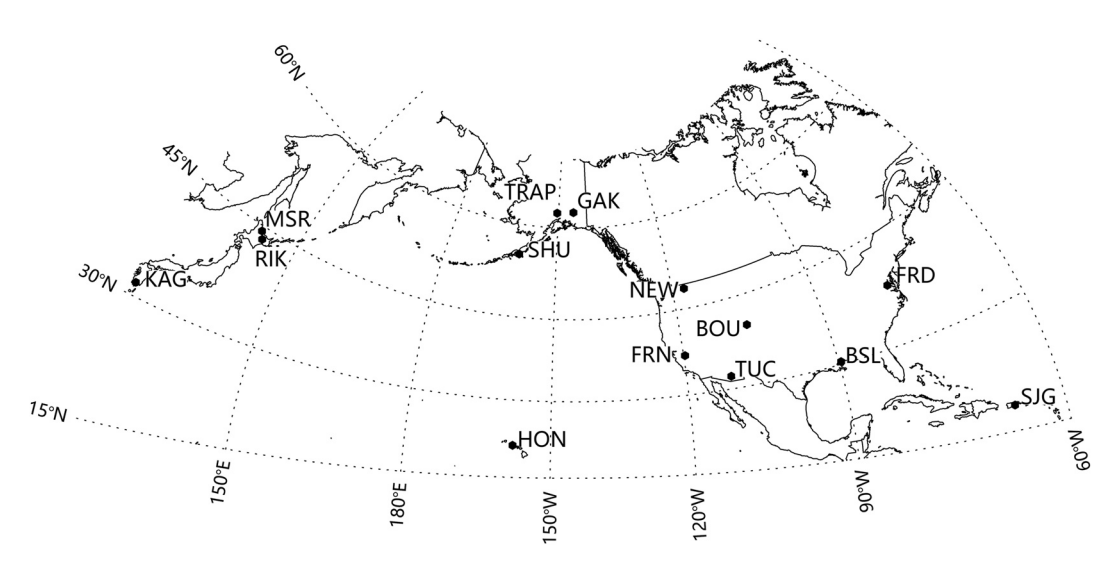


Figure 1. A map showing the location of auroral observation (GAK) and magnetometers measurements used in this study.

Exploration Agency (JAXA), and was launched on 20 December 2016. The Arase satellite is working on an orbit with 31° inclination, ~400-km altitude perigee and ~32,000-km altitude apogee (Miyoshi et al., 2018a). We used data from Low-Energy Particle experiments—ion mass analyzer (LEP-i, measuring 10 eV/q–25 keV/q ions) (Asamura, Kazama, et al., 2018), Medium-Energy Particle experiments—ion mass analyzer (MEP-i, measuring 10–180 keV/q ions) (Yokota et al., 2017), Low-Energy Particle experiments - electron analyzer (LEP-e, measuring 19 eV–20 keV electrons) (Kazama et al., 2017) and Medium-Energy Particle experiments—electron analyzer (MEP-e,measuring 7–87 keV electrons) (S. Kasahara et al., 2018) to analyze ions and electrons fluxes. To investigate the electromagnetic waves, we examined data obtained by Magnetic Field Experiment (MGF) (Matsuoka, Teramoto, Nomura, et al., 2018), High Frequency Analyzer (HFA) (Kumamoto et al., 2018) and Electric Field Detector (EFD) (Kasaba et al., 2017). The HFA and EFD are integrated in the Plasma Wave Experiment (PWE) (Y. Kasahara et al., 2018) on board the satellite. The time resolution of data from LEP-i, MEP-i, LEP-e, MEP-e, MGF, and EFD was 8 s and that from HFA was 1 s.

For the ground-based observation, we used an electron-multiplying charge-coupled device (EMCCD) camera that was operated at Gakona, Alaska (Hosokawa et al., 2021). This EMCCD camera is part of study of dynamical variation of particles and waves in the inner magnetosphere using ground-based network observations (PWING project) (Shiokawa et al., 2017). A broadband filter named BG3 is set on the top of the fisheye lens of this camera. This filter allows the light transmission at wavelengths of 300–500 nm and above 700 nm to suppress slow oxygen emissions at 557.7 and 630.0 nm. Though the sampling rate of this EMCCD camera is 100 Hz, we used reproduced quick-look images with a cadence of 10s provided by ERG Science Center (ERG-SC, https://ergsc.isee.nagoya-u.ac.jp/index.shtml.en) (Miyoshi et al., 2018b). In this study, we used the ground magnetometers data provided by ISEE magnetometer network (https://stdb2.isee.nagoya-u.ac.jp/magne/), U.S. Geological Survey (USGS) (Love & Finn, 2011) and THEMIS (Russell et al., 2008) geomagnetic networks.

## 3. Observations

Figure 1 shows the locations of the ground stations from which the magnetic field and optical data for this study were obtained. An all-sky camera used in the present study is located at Gakona, Alaska. A substorm brightening arc was observed at Gakona at ~0743 UT on 28 December 2018, as shown later. The magnetic field variations observed by ground magnetometers at southwest (Figures 2a–2f) and southeast (Figures 2g–2l) of Gakona are presented in Figure 2. Figures 2a–2l show the X- and Y- component magnetic field variations at Moshiri (MSR, Figures 2a and 2d), Rikubetsu (RIK, Figures 2b and 2e) and Kagoshima (KAG, Figures 2c and 2f), Colville (NEW, Figures 2g and 2j), Boulder (BOU, Figures 2k and 2l) and Fresno (FRN, Figures 2i and 2i), respectively. At the auroral brightening timing (~0743 UT), the X-component of the magnetic field observed in Japan varied almost consistently; they tended to steeply decay at ~0747 UT and show a clear negative bay for ~0747–0820 UT. The Y-component of the magnetic field in Japan was gradually increasing before and after the

CHEN ET AL. 3 of 17

elibrary.wiley.com/doi/10.1029/2023JA031648 by University Of Alaska Fairbanks, Wiley Online Library on [22/01/2024]. See the Terms i

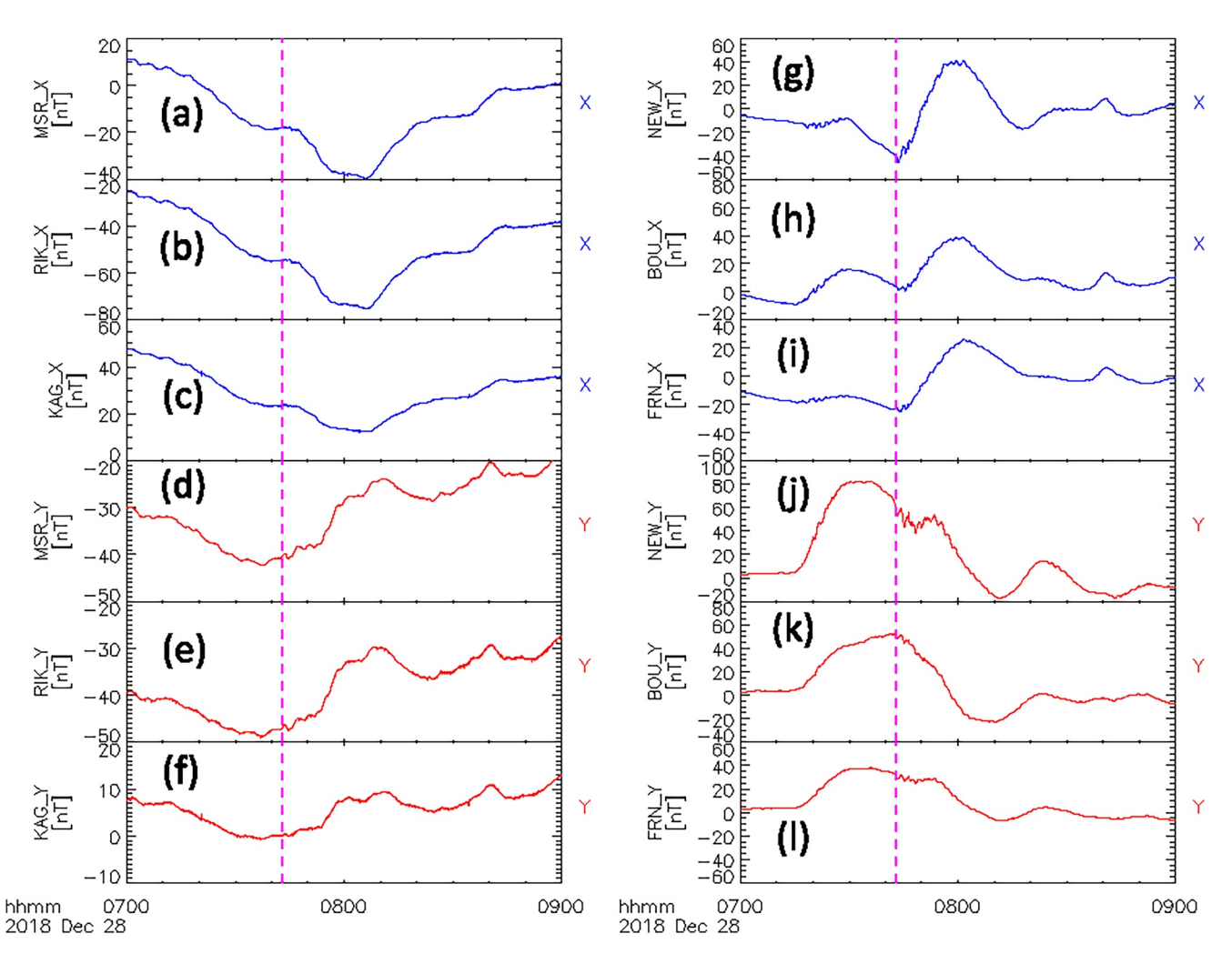


Figure 2. X-(blue) and Y-component (red) of the magnetic field variations observed at the southwest side of GAK (MSR, RIK, and KAG; left column), and at the southeast side of GAK (NEW, BOU, and FRN; right column).

auroral brightening at  $\sim 0730-0810$  UT. Around the west coast of America, the X-component of the magnetic field presents clear positive bay starting from 0743 UT to 0816 UT, while the Y-component tend to show a negative excursion before and after the substorm onset at  $\sim 0740-0810$  UT. These results indicate the formation of a SCW.

Figure 3 shows a sequence of auroral images between 0740 and 0804 UT on 28 December 2018, with 3 min cadence. These images were taken by an EMCCD camera with the BG3 filter operating at Gakona, Alaska (Shiokawa et al., 2017). Auroral video of the presented event is also provided in Movie S1. Figure 4 shows a north-south keogram made by clipping the auroral images along a meridional line that crosses the zenith at a longitude of 214.78°E. In these auroral images, it can be seen that an auroral arc was surging roughly from geographic southeast to northwest before the substorm onset. We note that the magnetic declination at Gakona is 18.31°. The auroral arc started to break-up at ~0743 UT, and azimuthally arraying fragments (commonly referred to auroral beads) appeared embedded in the arc intermittently when the aurora expanded northward before 0800 UT. After 0800 UT the auroral arc gradually diffused and vanished.

In Figure 3, the red dashed curves indicate the trajectory of the Arase satellite between 0720 and 0810 UT mapped from the inner magnetosphere to the ionosphere at an altitude of 100 km using the Tsyganenko 05 (TS05) model (Tsyganenko & Sitnov, 2005), and the yellow asterisk indicates the footprint of the Arase satellite at individual camera images. The Arase satellite was moving equatorward at the substorm onset and the in-situ measurement was made at the earthward side of the source region of the brightening arcs.

CHEN ET AL. 4 of 17

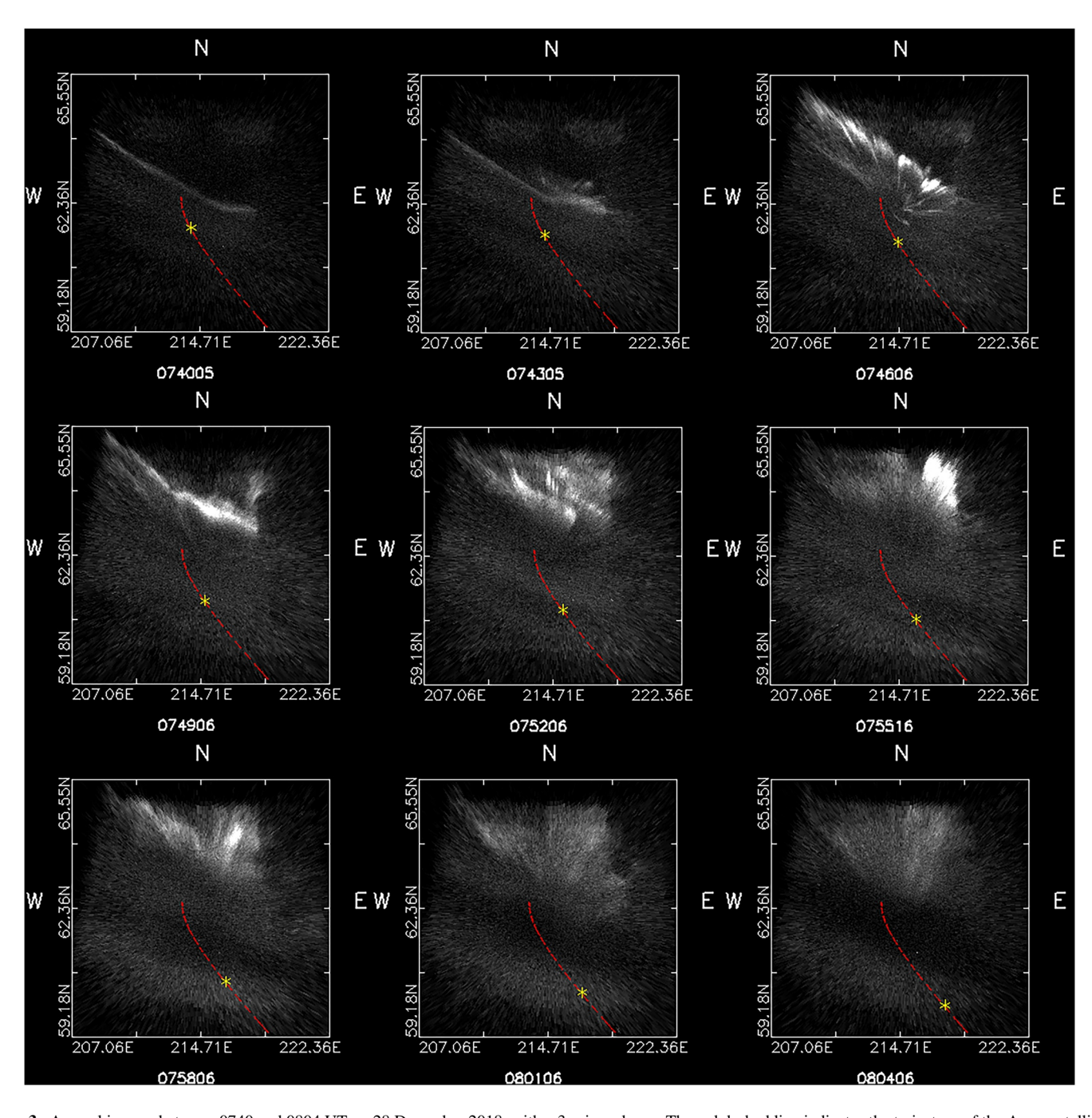
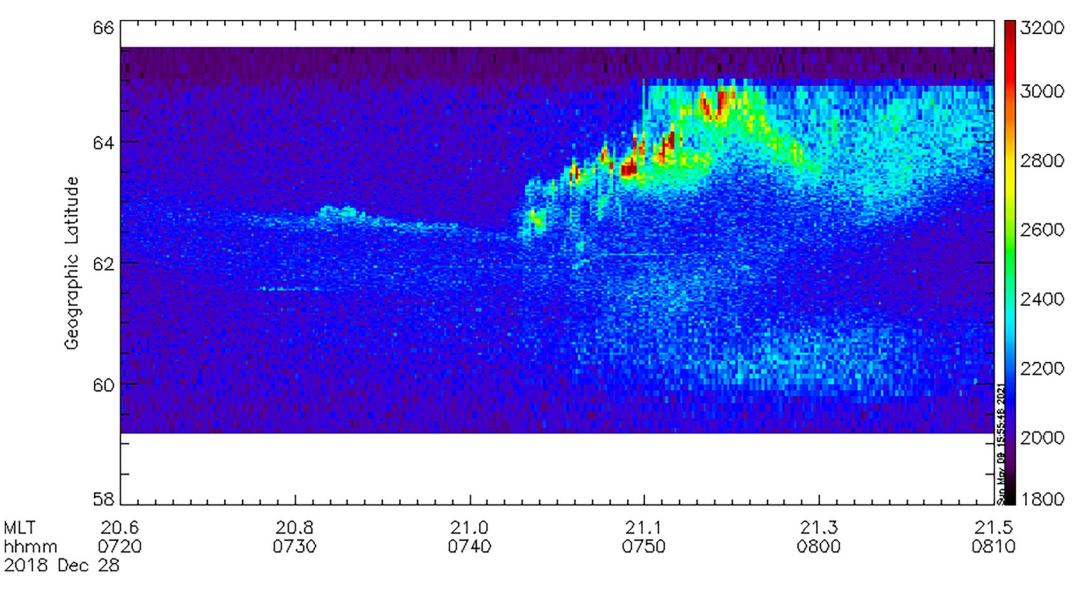


Figure 3. Auroral images between 0740 and 0804 UT on 28 December 2018, with a 3-min cadence. The red dashed line indicates the trajectory of the Arase satellite between 0720 and 0810 UT and yellow asterisk indicates the footprint of the Arase satellite mapped at an altitude of 100 km at individual camera images.

Another set of auroral images taken by THEMIS ASIs network is provided as Movie S2. It can be seen that the auroral arc break-up at the substorm onset was observed between  $\sim$ 200 and 260°E in geographic longitude, which indicates that the EMCCD camera at Gakona observed the western edge of the break-up aurora.

Figure 5 shows the X-component magnetograms obtained from stations close to Gakona (TRAP and SHU), and stations at mid- and low-latitudes in North America (NEW, BOU, FRD, FRN, TUC, and BSL), Honolulu (HON) and Cayey (SJG) during 0740–0800 UT. All panels in Figure 5 show the X-component variations with a fast Fourier transform (FFT) filter with a band pass window of 40–300 s. At stations close to Gakona, the X-component of the magnetic field was pulsating with a period of ~160 s, and the pulsation waveform at SHU

CHEN ET AL. 5 of 17



**Figure 4.** North-south keogram of auroral brightening reproduced from meridional cross section of the electron-multiplying charge-coupled device camera imagers at the longitude of Gakona (214.78°E).

(Figure 5b) was different from that at TRAP (Figure 5a). The amplitude of the perturbation at TRAP is larger. This difference may be due to the influence of auroral electrojet current variations considering that TRAP is closer to the auroral brightening region. The magnetic perturbations at high-latitude stations are clearly different from those at mid-latitude stations. In Figures 5c–5j, Pi2 frequency pulsation (period floating between ~70 and 100 s) is found at several mid-latitude stations between 18°N and 40°N. We draw red dashed lines to roughly indicate the variation peaks in these panels. It can be seen that perturbation peaks appear roughly simultaneously at different stations. The Pi2 waveform at these stations also present some latitudinal characteristics, where NEW, BOU, and FRD (Figures 5c–5e) variations are similar, while HON, FRN, TUC, BSL, and SJG present another similarity. These longitudinally extended mid- and low-latitude Pi2 pulsations are consistent with the cavity mode-type resonance, which is similar to the event reported by Keiling (2012).

Figure 6 shows the field and particle measurements made by the Arase satellite between 0730 and 0820 UT. Panels from top to bottom in Figure 6 are (a) the magnetic field in solar-magnetospheric (SM) coordinates, (b) electric field in SM coordinates, 40-300 s band-pass filtered perturbations in (c) magnetic and (d) electric field with a FFT filter, (e) Poynting flux in field-aligned coordinates, electron number flux spectra in (f) medium and (g) low energy ranges, and proton number flux spectra in (h) medium and (i) low energy ranges. On the bottom of Figure 6, labels of MLT, MLAT, R, and L-value denote the magnetic local time, magnetic latitude, radial distance and McIlwain's L-value of the satellite position, respectively. McIlwain's L-value is calculated based on the International Geomagnetic Reference Field model (Alken et al., 2021). The EFD on-board the Arase satellite can measure two components of the electric field in the spin plane of the satellite. The third component of the electric field in the spin axis direction is assumed based on the assumption of  $E \cdot B = 0$ . The ambient magnetic field had small angles with the spin plane during the present interval, which may lead to large ambiguity under this assumption when the magnetic field is parallel or anti-parallel to the measured electric field in the spin plane. We check the angle between the electric field in the spin plane and the magnetic field (not shown), and found that the angle was mostly  $\sim 60-120^{\circ}$  during 0740-0756 UT. This angle was far from parallel to the ambient magnetic field, indicating that the electric field component parallel to the magnetic field was fairly small and thus the field-aligned Poynting flux can be determined mostly from this measured electric field. After 0758 UT this angle became ~150°, more parallel to the magnetic field orientation, which could introduce a large uncertainty in the electric field component in the spin axis direction. The coordinate of the Poynting flux in Figure 6e is a field-aligned coordinate, where Z-axis is parallel to the ambient magnetic field and X-axis is in the plane formed by a vector pointing from the satellite to the earth and ambient magnetic field. The vertical dashed line indicates the reference time when the auroral arc started to breakup in the field-of-view (FOV) of the EMCCD camera at Gakona at 0743 UT.

CHEN ET AL. 6 of 17

21699402, 2023, 10, Downloaded from https://agupubs.onlinelibrary.wiley.com/doi/10.1029/2023JA031648 by University Of Alaska Fairbanks, Wiley Online Library on [22.01/2024]. See the Terms and Conditions (https://onlinelibrary.wiley.

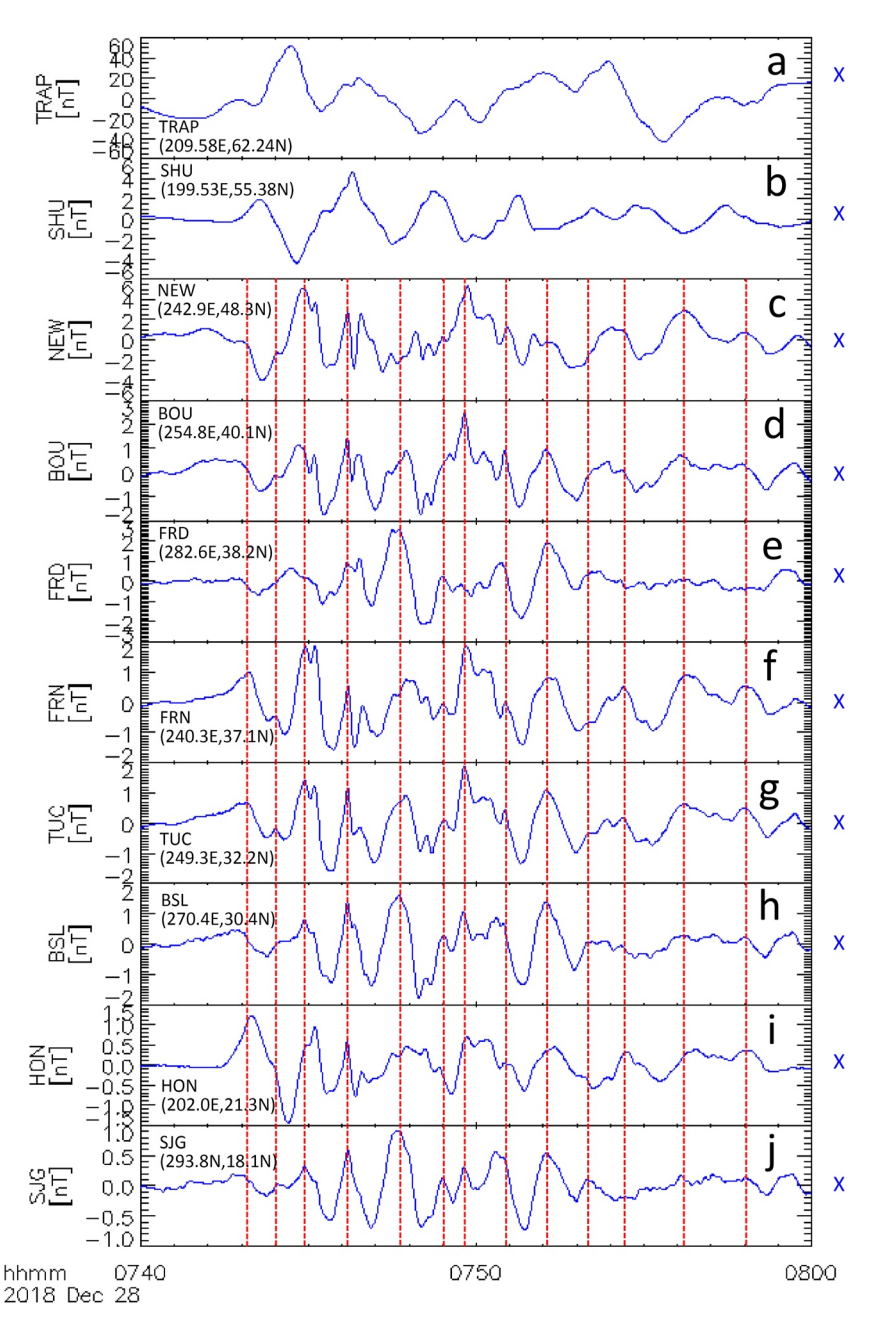


**Figure 5.** Ground-based observed fast Fourier transform filtered X-component magnetic field from the stations close to Gakona and stations at mid-latitude.

The Arase satellite was moving from  $L \sim 5$  to  $L \sim 4.6$  during 0740–0800 UT, with corresponding changes in magnetic latitude and MLT from 26.1° to 29.0° in the northern hemisphere and 21.0–21.6 MLT, respectively. During this time interval, the Arase satellite observed a series of electromagnetic variation and intensification in the proton and electron spectra. In Figures 6c and 6d the perturbation in magnetic field and electric field started at ~0741 UT, just before the auroral arc breakup. In Figure 6c, the magnetic field variation  $\delta B$  pulsated mainly in SM-x and SM-y components with a period of ~150 s during 0741–0749 UT, and its waveform became irregular after 0749 UT. In Figure 6d, the electric field variation  $\delta E$  was very similar to the magnetic field pulsation; it shows oscillations with a period of ~150 s and had a ~70–90° phase delay comparing with  $\delta Bx$  and  $\delta By$  during 0741–0749 UT. After 0749 UT, the waveform of  $\delta E$  also becomes much noisy. In the Poynting Flux panel of Figures 6e and 6a series of field-aligned enhancement of the Poynting flux (Sz) can be seen between 0741 and 0749 UT, during which 5 peaks and 4 troughs of energy flux were observed alternately. Except for the fifth peak

CHEN ET AL. 7 of 17

21699402, 2023, 10, Downloaded from https://agupubs.

onlinelibrary.wiley.com/doi/10.1029/2023JA031648 by University Of Alaska Fairbanks, Wiley Online Library on [22/01/2024]. See the Terms and Conditions (https://onlinelibrary.wiley

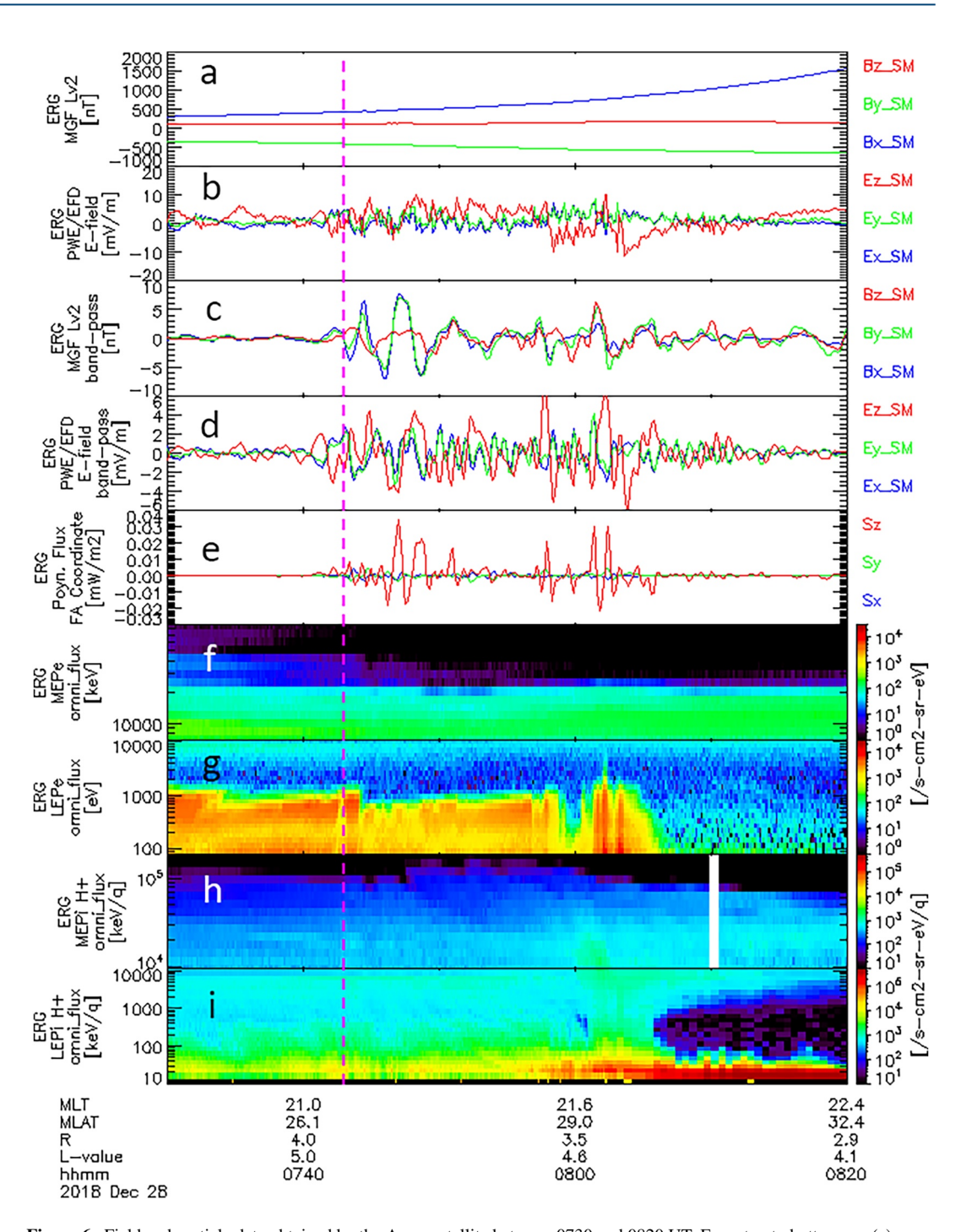


**Figure 6.** Field and particle data obtained by the Arase satellite between 0730 and 0820 UT. From top to bottom are (a) Magnetic field in solar-magnetospheric (SM) coordinate, (b) electric field in SM coordinate, (c) magnetic and (d) electric field perturbations with a 40–300 s band-pass fast Fourier transform filter, (e) Poynting flux in field-aligned coordinate, electron number flux spectra in (f) medium and (g) low energy ranges, proton number flux spectra in (h) medium and (i) low energy ranges.

at  $\sim$ 0749 UT which showed a small amount of Sx Poynting flux, most Poynting flux is field-aligned (Sz > Sx, Sy). It can be seen that the frequency of field-aligned Poynting flux intensification is roughly two times as high as the frequency in the electromagnetic waves. Considering that the Arase satellite was in the northern hemisphere, a positive value in Sz indicates the direction pointing from the equatorial plane of the magnetosphere to the ionosphere along the ambient magnetic field. The magnitude of the positive value in Poynting flux was larger than

CHEN ET AL. 8 of 17

elibrary.wiley.com/doi/10.1029/2023JA031648 by University Of Alaska Fairbanks, Wiley Online Library on [22/01/2024]. See the Terms and

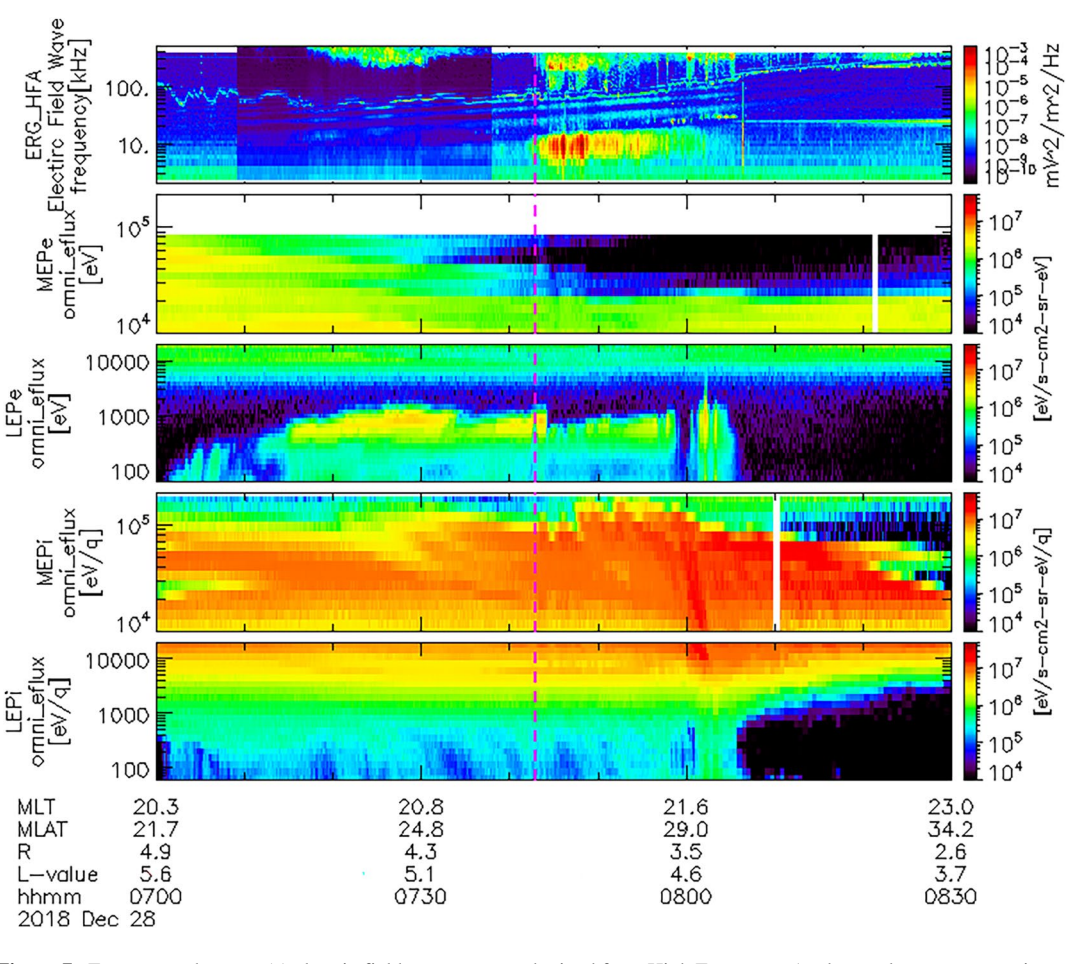


**Figure 7.** From top to bottom, (a) electric field wave spectra obtained from High Frequency Analyzer, electron energy-time spectra in (b) medium and (c) low energy ranges, and proton energy-time spectra in (d) medium and (e) low energy ranges, observed by the Arase satellite on 28 December 2018. Vertical dashed line indicates the timing of the auroral poleward expansion observed at Gakona.

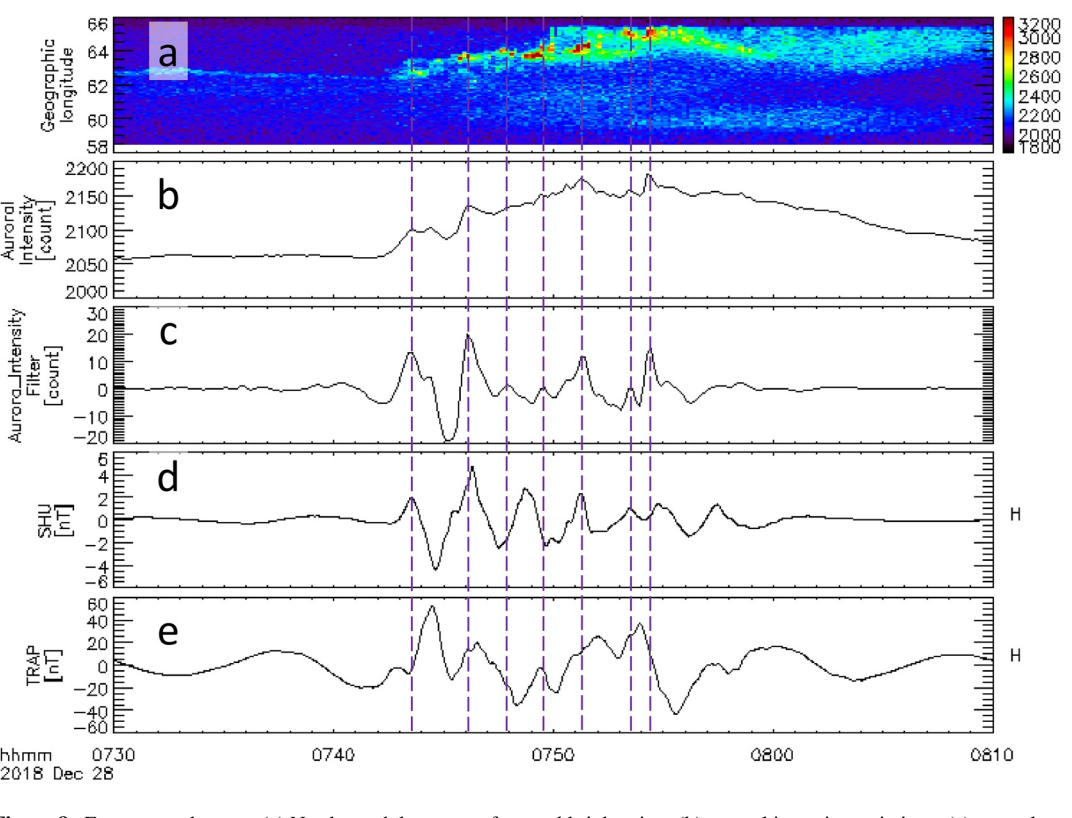
the negative, while the negative value is not negligible, indicating the existence of standing Alfven wave that is contained in the earthward flux. We note that the field-aligned Poynting flux after 0757 UT is not reliable because the corresponding electric field in the spin axis direction is ambiguous.

Figure 7 shows the (a) electric field wave spectra obtained from HFA, electron energy-time spectra in (b) medium and (c) low energy ranges, and proton energy-time spectra in (d) medium and low (e) energy ranges observed by the Arase satellite at 0700–0830 UT on 28 December 2018. In Figure 7a, an intensification of the waves at  $\sim$ 100–300 kHz and  $\sim$ 300–400 kHz can be seen at 1742–1752 UT and 1742–0805 UT, respectively. The frequency of these waves corresponds to that of the auroral kilometric radiations (AKRs), which probably manifest the field-aligned acceleration of electrons during substorms (e.g., Morioka and Miyoshi, 2012). As seen from the observations of the ground-all-sky camera in Figure 3, it can be seen that the appearance timing of the AKR at  $\sim$ 100–300 kHz corresponds to the timing of the auroral poleward expansion, which is consistent with previous studies (e.g., Morioka et al., 2010). In Figure 7a, another wave intensification can be seen at  $\sim$ 3–20 kHz at  $\sim$ 0742–0802 UT. This frequency roughly corresponded to one half of the local electron cyclotron frequency, indicating the existence of whistler mode waves near the auroral source region.

In Figures 7b–7e, it can be seen that the electron energy flux was distributed mostly in the range of  $\sim$ 3–90 keV at  $\sim$ 0700–0740 UT and  $\sim$ 3–30 keV at  $\sim$ 0740–0830 UT, while proton energy flux was mostly in the range of  $\sim$ 1–200 keV/q. In Figure 7c, however, electron energy flux at lower energies at  $\sim$ 100–1,000 eV can be also seen at  $\sim$ 0715–0805 UT. In Figures 7c and 7d, it has to be noted that the energy flux intensified intermittently after 0742 UT for 400–800 eV electrons and 70–200 keV/q protons, which may correlate with auroral intensification observed by the ground all-sky camera. We further examine these features in the discussion section.

CHEN ET AL. 9 of 17

brary.wiley.com/doi/10.1029/2023JA031648 by University Of Alaska Fairbanks, Wiley Online Library on [22/01/2024]. See the Terms and



**Figure 8.** From top to bottom, (a) North-south keogram of auroral brightening, (b) auroral intensity variations, (c) auroral intensity variations with a band-pass fast Fourier transform (FFT) filter, X-component magnetic field variations at (d) SHU and (e) TRAP with a band-pass FFT filter.

## 4. Detail Comparison and Discussion

In the previous sections, we have shown the observations made by a ground-based optical camera, ground magnetometers and data from the Arase satellite in terms of the relative timing between ground and magnetospheric signatures. In this section we examine the ground and satellite measurements to show their correlations in more detail.

Figure 8 shows the comparison of the auroral brightening and the high latitudinal Pi2 pulsations. Figure 8a shows the auroral keogram that is identical to that of Figure 4. Figure 8b shows the auroral intensity variations derived by averaging auroral intensities over the whole auroral images in geographical coordinates that are in Figure 3. Figure 8c shows the auroral intensity variation after applying a 40–300 s band-pass FFT filter to it. Figures 8d and 8e indicate the X-component variations of the high-latitude magnetic field at SHU and TRAP using the same 40–300 s band-pass FFT filter, which are the same as those shown in Figures 5a and 5b, respectively. Vertical dashed lines are drawn at the timings of intensification in the auroral luminosity presented in Figures 8a and 8c. Comparing these dashed lines with geomagnetic field in Figure 8, we can identify one-to-one correspondence between the auroral optical observation and the ground magnetometer measurement at SHU, where the 1st, 2nd, 5th, 6th, and 7th dash lines roughly match with the peaks of the X-component variations. Correspondence between the auroral luminosity and the X-component magnetic field variations at TRAP are not as evident, where only the 4th, and 6th lines could match. A previous study made by Keiling et al. (2008) report the one-to-one correspondence between Polar UVI auroral optical intensification and ground Pi2 pulsations, indicating that the SCW and additional current structure in the plasma sheet contribute to the modulations of substorm aurora. Another study made by Solovyev et al. (2000) suggested that high-latitude Pi2 is more likely to correlate with transient localized field-aligned current (FAC) enhancement rather than background SCW. Considering that TRAP is much closer to the auroral brightening region than SHU, and the amplitude of magnetic field variations at TRAP is an order of magnitude larger than that at SHU, we suggest that the magnetometer measurement at TRAP might be significantly affected by the background SCW and the associated auroral electrojet currents,

CHEN ET AL. 10 of 17

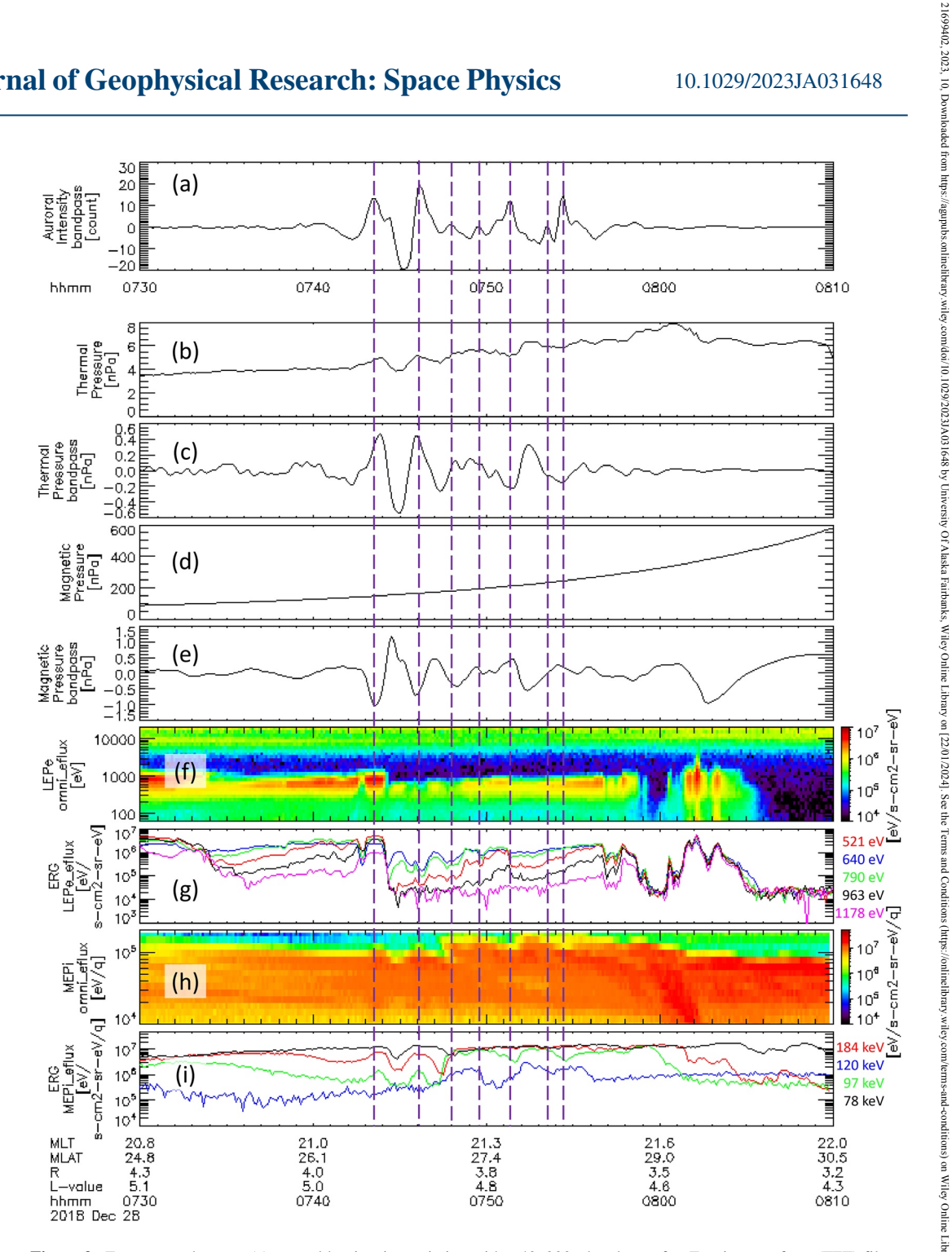


Figure 9. From top to bottom, (a) auroral luminosity variation with a 40–300 s band-pass fast Fourier transform (FFT) filter, (b) thermal pressure and (c) its oscillation with a 40-300 s band-pass FFT filter obtained from Arase, (d) magnetic pressure and (e) its oscillation with a 40-300 s band-pass FFT filter obtained from Arase, (f) energy-time spectra of electron energy flux obtained from LEP-e, (g) electron energy flux between 500 and 1,200 eV, (h) energy-time spectra of ion energy flux obtained from MEP-i, (i) ion energy flux between 70 and 200 keV.

while the Pi2 pulsations at SHU was a manifestation of the periodic FAC enhancement in the Pi2 frequency range, which contribute to auroral luminosity variations.

Figure 9 shows a detailed comparison between ground and the Arase satellite observations. Figures 9a show the auroral intensity variations (identical to Figures 8c), and Figures 9b-9i are based on the data from the Arase satellite. Figure 9b shows the non-filtered thermal pressure combining both MEP-i (H+, energy range between 26 and 185 keV/q) and LEP-i (H+, energy range between 10 and 26 keV/q) fluxes, and its oscillation with a 40-300s band-pass FFT filter is shown in Figure 9c. The magnetic pressure calculated from the MGF data

CHEN ET AL. 11 of 17 and its oscillation derived with a 40–300s band-pass FFT filter are shown in Figures 9d and 9e, respectively. Time-energy spectra of electron and ion energy fluxes from LEP-e and MEP-i are shown in Figures 9f and 9h, which are identical to Figures 7c and 7d. The electron energy flux at 500–1200 eV and ion energy flux at 70–200 keV, for which intermittent enhancements can be seen at 0743–0800 UT in the energy-time spectra in Figures 9f and 9h are shown in Figures 9g and 9i, respectively. The vertical dashed lines in Figure 9 are drawn at the timings of peaks in the aurora luminosity oscillation in Figure 9a.

Comparing the filtered variations of magnetic and thermal pressure in Figures 9c and 9e, we can see they show anti-phase variations, possibly indicating the slow mode wave transmission around the geosynchronous orbit (Miyashita et al., 2021). Keiling et al. (2008) suggest that such diamagnetic plasma oscillation is related to wave phenomena in the inner magnetosphere, such as ballooning mode instability. In Figures 9a and 9c, it can be seen that the aurora luminosity intensification roughly matches with the peaks of thermal pressure variation for the 1st, 2nd, 3rd, and 4th dashed lines. This correspondence can also be seen in the correspondence between ion energy flux enhancement and aurora luminosity, where ion energy flux increases roughly at 1st, 2nd, 3rd, and 4th dashed lines in Figure 9i in one or several energy channels. It is very interesting to emphasize that the electron energy flux in Figure 9g presents one-to-one correspondence between flux trough and aurora brightening peaks at 2nd, 3rd, 4th, and 5th dashed lines. Along with the ion energy flux panel, these results imply electron and ion energy flux intensified alternately near the source region of the substorm brightening arc in the inner magnetosphere. Such oscillation is similar with the picture of ballooning mode instability, where excess electrons and ions are accumulated on both sides of tail-like stretched magnetic field line (Roux et al., 1991). Thus, the oscillations in the magnetic field and particle energy flux observed by satellite as well as their correspondence with the auroral luminosity variation strongly suggest the occurrence of ballooning mode instability in the source region of substorm brightening aurora.

Figure 10 shows the periodograms of several observational data during 0730–0810 UT presented in this study. These periodograms are reproduced by FFT, where the amplitude at each frequency is the average over  $\pm 2$  adjacent discrete frequencies. Figure 10a shows the periodogram of high latitudinal ground-based observations and the satellite measurement, including the X-component of the magnetic field at SHU, auroral luminosity variation observed at Gakona, and the magnetic and electric field as well as thermal pressure measured by the Arase satellite. Figure 10b shows the periodograms of the X-component of the magnetic field at mid- and low-latitude stations which are shown in Figures 5c-5j.

In Figure 10a, the periodograms show slight enhancements at  $\sim$ 4.17–8.75 mHz in the X-component of the magnetic field at SHU and the electric field, magnetic field, and thermal pressure from Arase. A dashed line is drawn at 6.67 mHz, which is referred to a rough median frequency of the enhancements. The periodograms of auroral intensity show intensification at  $\sim$ 3.33–7.08 mHz, although the low-frequency part of these enhancements, for example, about 3.33 mHz (300 s period), is not clear in its waveform in Figure 8b.

In Figure 10b, the X-component of the magnetic field at mid- and low-latitudes show peaks at  $\sim 11.25$ ,  $\sim 14.58$ , and 17.08 mHz in the stations except for NEW, HON, and FRN. The periodograms from NEW, HON and FRN show enhancements at  $\sim 5.42-11.67$  mHz, 14.17 and 17.08 mHz. Enhancements at  $\sim 11$  mHz ( $\sim 90$  s period) are shown at most stations, which are consistent with the Pi2 waveforms shown in Figure 5. Enhancements at  $\sim 7$  mHz ( $\sim 140$  s period) can be seen in the periodograms of many stations, which may indicate their correlations with the variations measured at high-latitudes and by Arase at similar frequencies. Nevertheless, the waveform of magnetic field at mid- and low-latitudes present neither clear perturbations at this frequency in Figure 5, nor correspondences with the measurements at high-latitude.

The dominant frequency is different between high-latitude and satellite observations and mid-latitude observations, indicating that the waves observed at high- and mid-latitude stations may come from different sources. As we suggest in the previous discussion,  $\sim$ 11 and  $\sim$ 14 mHz Pi2 pulsations observed at mid-latitude stations could probably be caused by a cavity-type PCR or PVR, while the satellite was located outside of the plasmapause and might not observe significant magnetic field oscillation at these frequencies. Here, if we regard 11.25 mHz wave as the fundamental mode wave and 14.58 mHz wave as the second harmonic, the ratio between these two frequencies is  $\sim$ 1.30, which is smaller than previous studies made by Denton et al. (2002) ( $\sim$ 1.8) and Cheng et al. (2000) ( $\sim$ 1.7).

Field-aligned acceleration of electrons occurs frequently during auroral substorms and contributes to the formation and modulation of substorm auroral brightening. One mechanism for field-aligned acceleration is known as

CHEN ET AL. 12 of 17

21699402, 2023, 10, Downloaded from https://agupubs.onlinelibrary.wiley.com/doi/10.1029/2023JA031648 by University Of Alaska Fairbanks, Wiley Online Library on [22/01/2024]. See the Terms and Conditions (https://agupubs.onlinelibrary.wiley.com/doi/10.1029/2023JA031648 by University Of Alaska Fairbanks, Wiley Online Library on [22/01/2024]. See the Terms and Conditions (https://agupubs.onlinelibrary.wiley.com/doi/10.1029/2023JA031648 by University Of Alaska Fairbanks, Wiley Online Library on [22/01/2024]. See the Terms and Conditions (https://agupubs.onlinelibrary.wiley.com/doi/10.1029/2023JA031648 by University Of Alaska Fairbanks, Wiley Online Library on [22/01/2024]. See the Terms and Conditions (https://agupubs.onlinelibrary.wiley.com/doi/10.1029/2023JA031648 by University Of Alaska Fairbanks, Wiley Online Library on [22/01/2024]. See the Terms and Conditions (https://agupubs.onlinelibrary.wiley.com/doi/10.1029/2023JA031648 by University Of Alaska Fairbanks, Wiley Online Library.wiley.com/doi/10.1029/2023JA031648 by University

**Figure 10.** Periodograms of (a) ground-based high-latitude observations and the Arase satellite measurement, and (b) X-component magnetic field variations observed at mid- and low-latitude stations. The units in the vertical axis of (a) are nT<sup>2</sup>/Hz (ERG-B and SHU), mV<sup>2</sup>/m<sup>2</sup>/Hz (ERG-E), nPa<sup>2</sup>/Hz ( $P_{th}$ ) and count<sup>2</sup>/Hz (aurora), respectively.

quasi-static potential acceleration, which was confirmed by FAST observation made by McFadden et al. (1999). Recently another observation made by Tian et al. (2021) presented one-to-one correlation between Poynting flux measured by RBSP and discrete aurora intensity observed by all-sky camera, suggesting that electron acceleration was carried out by kinetic Alfven wave. In the present event, the wave spectrum of electric field in Figure 7a shows AKR during auroral brightening poleward expansion. We integrated the electric field wave intensity between 100 and 1,000 kHz in Figure 7a during 0700-0830 UT (not shown) and compare it with the auroral luminosity. However, we did not find clear one-to-one correspondence between integrated electric wave intensity and the aurora luminosity variations. From the Arase satellite data, we can estimate the local Alfven velocity using the formula  $V_A = B/(nm\mu_0)^{1/2}$ , where n is the local plasma density, m is the ion mass, and  $\mu_0$  is the permeability of vacuum. We estimate the local Alfven velocity at the satellite position to be  $\sim$ 1800 km/s for  $B \sim 700$  nT and  $n \sim 70 \text{ cm}^{-3}$  (determined from UHR frequency measured by Arase). Considering the distance between Arase location (~4 Re) and the earth, it would take ~20 s for MHD wave to travel from the satellite to the ionosphere. In Figure 9, however, no significant delay can be found between the variations at the satellite and the aurora brightening variation. These observational results indicate that while field-aligned electron acceleration probably contributed to the formation of the observed substorm auroral brightening and background FAC, the modulations of auroral luminosity was not correlated with the observed signature of field-aligned acceleration. Thus, we suggest that the auroral brightening variations at Pi2 period in this event were probably caused by direct precipitation of electrons with kilo-electronvolt energies injected from the tail in association with substorms rather than

CHEN ET AL. 13 of 17

field-aligned accelerations, though we need to note that the weak signatures of the field-aligned accelerations from observations might be due to slight deviation between the satellite footprint and the auroral brightening. Considering that the period of the electromagnetic waves observed by Arase was consistent with that of auroral luminosity variations, we suggest that the precipitating electrons were probably modulated through Alfven waves.

It is also argued that Pi2 pulsations observed on the ground during auroral substorm is directly driven by quasi-periodic earthward BBF in the plasma sheet (Kepko et al., 2001; Nishimura et al., 2012). Kepko et al. (2001) examined six BBF events at 8 and 15 Re in the magnetotail using the Geotail satellite and identified one-to-one correspondences between ground-based Pi2 and earthward plasma flow enhancements in the magnetotail. Nishimura et al. (2012) presented a multi-event study regarding the auroral intensifications during substorm expansion phase using THEMIS ASIs. In their study, Pi2 pulsations were observed from the auroral oval latitudes to equatorial stations, and the latitudinally distributed Pi2 pulsations show a frequency similar to that of auroral poleward intensifications. In their events, auroral intensifications tend to anti-correlate with Pi2 pulses at the auroral region and correlate with mid-low latitude Pi2 pulsations, where they conclude that this Pi2 feature manifests the existence of oscillating current wedge that is directly driven by earthward busty flows at a Pi2 frequency. In the present event, however, pulsations in the X-component of the magnetic field at the mid- and low-altitude stations apparently oscillated neither at the same frequency nor with the same waveform as that at high latitudes, indicating that high-latitudinal Pi2 originated from a different source.

We also checked the variation in ion bulk velocity estimated from the data obtained by the Arase satellite (not shown). The Ion velocity estimated from MEP-i was fluctuating between  $\sim \pm 100$  km/s at a very high frequency, indicating that MEP-i was significantly affected by a low count rate of MEP-i. Nevertheless, the value of  $\pm 100$  km/s is much smaller than the typical speed of BBFs at radial distances outside of 10 Re (e.g., Angelopoulos et al., 1992, 1996,  $\sim 500$  km/s). A similar result was shown in the velocity estimated from the LEP-i measurement where the ion velocity varies between  $\sim \pm 30$  km/s. LEP-i may not provide reliable values for such a small velocity measurement because of a low count rate. The EMCCD images from Gakona also did not provide any evidence of auroral streamer related to BBFs. There is a possibility that the BBFs took place at a location further tailward or at another magnetic local time and created relevant wave phenomena during the preconditioning of the substorm (e.g., Panov et al., 2010, 2014). Thus, we cannot verify or exclude this possibility because in this study we do not have the data to build a correlation between BBFs observed by satellites in the magnetotail and auroral luminosity on the ground.

In Figure 7d, several energy/time-dispersed characteristics can be seen in the proton energy flux spectrogram, that is, dispersed dropouts of energy flux from ~0722 UT to ~0740 UT between 22.1 and 149.8 keV, and dispersed enhancements of energy flux from  $\sim$ 0752 UT to  $\sim$ 0758 UT between 27.3 and 97.3 keV and from  $\sim$ 0758 UT to 0802 UT between 9.6 and 120.4 keV. Usually, an energy/time-disperseless particle injection indicates that the satellite is located within the injection local time, while a dispersive injection indicates that observation is made longitudinally distant from the source of injection, because of the different westward (eastward) drift velocities of ions (electrons) with different energies (Cohen et al., 2019). Energy/time-dispersive flux of protons and electrons has been reported in previous studies (e.g., Reeves et al., 1990; Turner et al., 2017), Reeves et al. (1990) estimated the angular drift velocities of differential protons with 110–380 keV around the geosynchronous orbit, where, for example, the angular drift velocity of protons with 110 keV is  $\sim 0.091^{\circ}$  per second. In the present event, the Arase satellite was moving from  $L \sim 6.63$  to  $L \sim 5.21$  at 0720 UT to 0800 UT when projected to the magnetic equatorial plane using the TS05 model. Given that the drift velocity of protons is proportional to its energy and applying the result from Reeves et al. (1990), we estimate that the injection regions of the dispersive energy flux enhancements during ~0752–0758 UT and during  $\sim 0.0758 - 0.0802$  UT might be  $\sim 11^{\circ}$  and  $\sim 2^{\circ}$  eastward of the satellite, respectively. It is interesting to note that though dispersive flux dropouts of electrons have been reported (e.g., Sergeev et al., 1992; Cohen et al., 2019), the dispersive flux dropouts of protons during ~0722–0740 UT has not been reported yet. Using the same method above, we estimate the injection region of this "drifting ion hole" to be  $\sim 23^{\circ}$  eastward of the satellite, which might correspond to an earlier substorm aurora at ~0716 UT to the east of Gakona (see Movie S2). To further investigate their relation needs observations at corresponding local times, which is beyond the object of our study.

# 5. Conclusions

In this paper, we study an auroral substorm event that took place over Gakona, Alaska on 28 December 2018. This is a comprehensive analysis of plasma and field variations at  $L \sim 4-5$  in the inner magnetosphere at substorm onset, showing correspondence of wave phenomena in the Pi2 frequency range between ground and satellites

CHEN ET AL. 14 of 17

near the magnetospheric source of the auroral brightening. The results and implications from the present event are summarized as follows.

- 1. The EMCCD camera on the ground observed poleward expansion of substorm auroral brightening at  $\sim$ 0743 UT, while the ionospheric footprint of the Arase satellite was moving southeastward at the south of the brightening aurora. High-latitude magnetometers observed oscillations in the X-component with a period of  $\sim$ 160 s at the onset of auroral brightening and poleward expansion, while mid- and low-latitude stations observed Pi2 pulsations with  $\sim$ 70–100 s periods.
- 2. From the Arase satellite at L ~ 4-5, we found magnetic and electric field fluctuations with a ~150 s period from ~0741 UT. The electric field wave showed a ~70-90° phase delay from the magnetic field wave during ~0741-0749 UT. They provide field-aligned Poynting flux intensification with frequencies of roughly two times higher than the frequency in the electromagnetic waves. These observations indicate the existence of the standing Alfven waves, which were probably excited by the substorm activity close to the Arase satellite.
- 3. Comparing the Arase satellite and ground observations, we found that magnetic and thermal pressures, electron energy flux at 500-1,200 eV, ion energy flux at 70-200 keV, auroral luminosity, and high-latitudinal magnetic field pulsation fluctuated roughly with the same frequency of ~6 mHz. Their correspondence was apparent especially during the first 10 min after the substorm onset and poleward expansion at 0743 UT. These observational results support the scenario that the wave phenomena in the inner magnetosphere modulate the substorm auroral intensity. We suggest that ballooning instability was likely to have a close relation to these wave phenomena, and the potential contribution of BBF at further tailward is difficult to evaluate.
- 4. Because no clear delay was found between satellite-measured Alfven waves and ground auroral luminosity and magnetic field variations, we suggest that the auroral intensity variation was directly caused by modulation of kilo-electronvolt electron precipitation through Alfven waves.

It has been widely suggested that substorm-related phenomena are triggered somewhere near the magnetic equatorial plane. Recently the simulation by Ebihara and Tanaka (2015) indicate that substorm initial auroral brightening is triggered by plasma vortices in the off-equatorial region in the inner-magnetosphere. In the present event, despite that the Arase satellite was located at a high magnetic latitude (~26 Mlat), we cannot address whether the observed wave phenomena come from the magnetic equator or not, because Alfven/slow mode waves can propagate along magnetic field lines. Meanwhile, the ground and in-situ magnetospheric wave phenomena during auroral substorm does not always show correspondence (e.g., Chen et al., 2022). This may indicate that some other mechanisms may take part in the moderation of substorm auroral brightening. Further observations are necessary to answer these questions.

# **Data Availability Statement**

The scientific data from the ERG (Arase) satellite was obtained from the ERG-SC operated by ISAS/JAXA and ISEE/Nagoya University (https://ergsc.isee.nagoya-u.ac.jp/index.shtml.en; Miyoshi et al., 2018b). This study analyzed LEP-e-L2 omniflux v03\_01 data (Wang, S. et al., 2018a), LEP-e-L2 3dflux v03\_01 data (Wang, S. et al., 2018b), LEP-i-L2 omniflux v03\_00 data (Asamura et al., 2018b), LEP-i-L2 3dflux v03\_00 (Asamura et al., 2018c), MEP-e-L2 omniflux v01\_02 data (S. Kasahara et al., 2018), MEP-e-L2 3dflux v01\_01 data (S. Kasahara et al., 2018), MEP-i-L2 omniflux v02\_01 data (Yokota et al., 2018a), MEP-i-L2 3dflux v01\_03 data (Yokota et al., 2018b), PWE/EFD/L2-E\_spin v05\_01 data (Y. Kasahara et al., 2018), PWE/HFA-L2 v01\_02 (Y. Kasahara et al., 2018), MGF-L2 8s v03.04 data (Matsuoka, Teramoto, Imajo, et al., 2018), and L2 v03 orbit data (Miyoshi et al., 2018c). The optical data from the Gakona station is available from the ISEE through the ERG-SC. The PWING observation data can also be obtained from the ERG-SC. The magnetometer data of USGS and THEMIS geomagnetic networks can be obtained through Coordinated Data Analysis Web (CDAWeb, https://cdaweb.gsfc.nasa.gov/index.html). The magnetometer data of ISEE magnetometer network can be obtained through the ERG-SC. The solar wind parameters and W-parameters used in the TS05 model were provided by the TS05 web repository (http://geo.phys.spbu.ru/~tsyganenko/TS05\_data\_and\_stuff/).

CHEN ET AL. 15 of 17

Acknowledgments

We thank Y. Yamamoto, and T. Adachi of ISEE, Nagoya University for their continuous support of the all-sky imager operation. This work was supported by Grants-in-Aid for Scientific Research (15H05815 (Y. Miyoshi), 16H06286 (K. Shiokawa), 20H01959 (Y. Miyoshi); 22K21345 (K. Shiokawa), 22H01283 (S. Oyama), 21KK0059 (K. Hosokawa), 22H00173(K. Hosokawa)) and core-tocore program (JPJSCCB20210003, K. Shiokawa) from the Japan Society for the Promotion of Science. L. C. is financially supported by China Scholarship Council (CSC) for his Doctoral course study. A part of work of S.O. was carried out by the joint research program of Planetary Plasma and Atmospheric Research Center, Tohoku University. Most of the data analysis was conducted using the Space Physics Environment Data Analysis Software (SPEDAS) tool (Angelopoulos

#### References

Journal of Geophysical Research: Space Physics

- Alken, P., Thébault, E., Beggan, C. D., Amit, H., Aubert, J., Baerenzung, J., et al. (2021). International geomagnetic reference field: The thirteenth generation. Earth Planets and Space, 73(1), 49. https://doi.org/10.1186/s40623-020-01288-x
- Angelopoulos, V., Baumjohann, W., Kennel, C. F., Coroniti, F. V., Kivelson, M. G., Pellat, R., et al. (1992). Bursty bulk flows in the inner central plasma sheet. Journal of Geophysical Research, 97(A4), 4027-4039. https://doi.org/10.1029/91ja02701
- Angelopoulos, V., Coroniti, F. V., Kennel, C. F., Kivelson, M. G., Walker, R. J., Russell, C. T., et al. (1996). Multipoint analysis of a bursty bulk flow event on April 11, 1985. Journal of Geophysical Research, 101(A3), 4967-4989. https://doi.org/10.1029/95JA02722
- Angelopoulos, V., Cruce, P., Drozdov, A., Grimes, E. W., Hatzigeorgiu, N., King, D. A., et al. (2019). The space physics environment data analysis system (SPEDAS) [Software]. Space Science Reviews, 215, 9. https://doi.org/10.1007/s11214-018-0576-4
- Asamura, K., Kazama, Y., Yokota, S., Kasahara, S., & Miyoshi, Y. (2018). Low-energy particle experiments-ion mass analyzer (LEPi) onboard the ERG (Arase) satellite. Earth Planets and Space, 70(1), 70. https://doi.org/10.1186/s40623-018-0846-0
- Asamura, K., Miyoshi, Y., & Shinohara, I. (2018b), The LEPi instrument Level-2 omniflux data of exploration of energization and radiation in geospace (ERG) Arase satellite [Dataset]. ERG. https://doi.org/10.34515/DATA.ERG-05001
- Asamura, K., Miyoshi, Y., & Shinohara, I. (2018c). The LEPi instrument Level-2 3D flux data of exploration of energization and radiation in geospace (ERG) Arase satellite [Dataset]. ERG. https://doi.org/10.34515/DATA.ERG-05000
- Chen, L., Shiokawa, K., Miyoshi, Y., Oyama, S., Jun, C.-W., Ogawa, Y., et al. (2022). Observation of source plasma and field variations of a substorm brightening aurora at  $L \sim 6$  by a ground-based camera and the Arase satellite on 12 October 2017. *Journal of Geophysical Research*: Space Physics, 127(11), e2021JA030072. https://doi.org/10.1029/2021JA030072
- Cheng, C.-C., Chao, J.-K., & Yumoto, K. (2000). Spectral power of low-latitude Pi2 pulsations at the 210° magnetic meridian stations and plasmaspheric cavity resonances. Earth Planets and Space, 52(9), 615-627. https://doi.org/10.1186/bf03351670
- Cohen, I. J., Mauk, B. H., Turner, D. L., Fennell, J. F., Blake, J. B., Reeves, G. D., et al. (2019). Drift-dispersed flux dropouts of energetic electrons observed in Earth's middle magnetosphere by the Magnetospheric Multiscale (MMS) mission. Geophysical Research Letters, 46(6), 3069-3078. https://doi.org/10.1029/2019GL082008
- Denton, R. E., Lee, D. H., Takahashi, K., Goldstein, J., & Anderson, R. (2002). Quantitative test of the cavity resonance explanation of plasmaspheric Pi2 frequencies. Journal of Geophysical Research, 107(A7), 1093. https://doi.org/10.1029/2001ja000272
- Ebihara, Y., & Tanaka, T. (2015). Substorm simulation: Formation of westward traveling surge. Journal of Geophysical Research: Space Physics, 120(12), 10466-10484. https://doi.org/10.1002/2015JA021697
- Hosokawa, K., Oyama, S. I., Ogawa, Y., Miyoshi, Y., Kurita, S., Teramoto, M., et al. (2021). A ground-based instrument suite for integrated high-time resolution 212 measurements of pulsating aurora with Arase. Earth and Space Science Open Archive, 213. https://doi.org/10.1002/
- Kasaba, Y., Ishisaka, K., Kasahara, Y., Imachi, T., Yagitani, S., Kojima, H., et al. (2017). Wire probe antenna (WPT) and electric field detector (EFD) of plasma wave experiment (PWE) aboard the Arase satellite: Specifications and initial evaluation results. Earth Planets and Space, 69(1), 174. https://doi.org/10.1186/s40623-017-0760-x
- Kasahara, S., Yokota, S., Hori, T., Keika, K., Miyoshi, Y., & Shinohara, I. (2018b). The MEP-e instrument Level-2 omni-directional flux data of Exploration of energization and Radiation in Geospace (ERG) Arase satellite [Dataset]. ERG. https://doi.org/10.34515/DATA.ERG-02001
- Kasahara, S., Yokota, S., Hori, T., Keika, K., Miyoshi, Y., & Shinohara, I. (2018c), The MEP-e instrument Level-2 3-D flux data of Exploration of energization and Radiation in Geospace (ERG) Arase satellite [Dataset]. ERG. https://doi.org/10.34515/DATA.ERG-02000
- Kasahara, S., Yokota, S., Mitani, T., Asamura, K., Hirahara, M., Shibano, Y., & Takashima, T. (2018a). Medium-energy particle experiments— Electron analyzer (MEP-e) for the exploration of energization and radiation in geospace (ERG) mission. Earth Planets and Space, 70(1), 69. https://doi.org/10.1186/s40623-018-0847-z
- Kasahara, Y., Kasaba, Y., Kojima, H., Yagitani, S., Ishisaka, K., Kumamoto, A., et al. (2018a). The plasma wave experiment (PWE) onboard the Arase (ERG) satellite. Earth Planets and Space, 70(1), 86. https://doi.org/10.1186/s40623-018-0842-4
- Kasahara, Y., Kasaba, Y., Matsuda, S., Shoji, M., Nakagawa, T., Ishisaka, K., et al. (2018b). The PWE/EFD instrument Level-2 spin-averaged potential data of exploration of energization and radiation in geospace (ERG) Arase satellite [Dataset]. ERG. https://doi.org/10.34515/DATA.
- Kasahara, Y., Kumamoto, A., Tsuchiya, F., Matsuda, S., Shoji, M., Nakamura, S., et al. (2018c). The PWE/HFA instrument Level-2 spectrum data of exploration of energization and radiation in geospace (ERG) Arase satellite [Dataset]. ERG. https://doi.org/10.34515/DATA.ERG-10000
- Kazama, Y., Wang, B. J., Wang, S. Y., Ho, P. T. P., Tam, S. W. Y., Chang, T. F., et al. (2017). Low-energy particle experiments-electron analyzer (LEPe) onboard the Arase spacecraft. Earth Planets and Space, 69(1), 165. https://doi.org/10.1186/s40623-017-0748-6
- Keiling, A. (2012). Pi2 pulsations driven by ballooning instability. Journal of Geophysical Research, 117(A3), A03228. https://doi. org/10.1029/2011JA017223
- Keiling, A., Angelopoulos, V., Larson, D., McFadden, J., Carlson, C., Fillingim, M., et al. (2008). Multiple intensifications inside the auroral bulge and their association with plasma sheet activities. Journal of Geophysical Research, 113(A12), A12216. https://doi.org/10.1029/2008JA013383
- Keiling, A., Fujimoto, M., Hasegawa, H., Honary, F., Sergeev, V., Semenov, V. S., et al. (2006). Association of Pi2 pulsations and pulsed reconnection: Ground and cluster observations in the tail lobe at 16RE. Annales Geophysicae, 24(12), 3433-3449. https://doi.org/10.5194/
- Keiling, A., Marghitu, O., Vogt, J., Amm, O., Bunescu, C., Constantinescu, V., et al. (2014). Magnetosphereionosphere coupling of global Pi2 pulsations. Journal of Geophysical Research: Space Physics, 119(4), 2717-2739. https://doi.org/10.1002/2013JA019085
- Kepko, L., Kivelson, M. G., & Yumoto, K. (2001). Flow bursts, braking, and Pi2 pulsations. Journal of Geophysical Research, 106(A2), 1903-1915. https://doi.org/10.1029/2000ja000158
- Kumamoto, A., Tsuchiya, F., Kasahara, Y., Kasaba, Y., Kojima, H., Yagitani, S., et al. (2018). High frequency analyzer (HFA) of plasma wave experiment (PWE) onboard the Arase spacecraft. Earth Planets and Space, 70(1), 82. https://doi.org/10.1186/s40623-018-0854-0
- Lester, M., Hughes, W. J., & Singer, H. J. (1984). Longitudinal structure in Pi2 pulsations and the substorm current wedge. Journal of Geophysical Research, 89(A7), 5489-5494. https://doi.org/10.1029/JA089iA07p05489
- Love, J. J., & Finn, C. A. (2011). The USGS geomagnetism program and its role in space weather monitoring. Space Weather, 9(7), S07001. https://doi.org/10.1029/2011SW000684
- Matsuoka, A., Teramoto, M., Imajo, S., Kurita, S., Miyoshi, Y., & Shinohara, I. (2018). The MGF instrument Level-2 spin-averaged magnetic field data of Exploration of energization and Radiation in Geospace (ERG) Arase satellite [Dataset]. ERG. https://doi.org/10.34515/DATA.
- Matsuoka, A., Teramoto, M., Nomura, R., Nosé, M., Fujimoto, A., Tanaka, Y., et al. (2018). The ARASE (ERG) magnetic field investigation. Earth Planets and Space, 70(1), 43. https://doi.org/10.1186/s40623-018-0800-1

CHEN ET AL. 16 of 17

- McFadden, J. P., Carlson, C. W., & Ergun, R. E. (1999). Microstructure of the auroral acceleration region as observed by FAST. *Journal of Geophysical Research*, 104(A7), 14453–14480. https://doi.org/10.1029/1998JA900167
- Miyashita, Y., Chang, T.-F., Miyoshi, Y., Hori, T., Kadokura, A., Kasahara, S., et al. (2021). Magnetic field and energetic particle flux oscillations and high-frequency waves deep in the inner magnetosphere during substorm dipolarization: ERG observations. *Journal of Geophysical Research: Space Physics*, 126(9), e2020JA029095. https://doi.org/10.1029/2020JA029095
- Miyoshi, Y., Hori, T., Shoji, M., Teramoto, M., Chang, T. F., Matsuda, S., et al. (2018b). The ERG science center. Earth Planets and Space, 70(1), 96. https://doi.org/10.1186/s40623-018-0867-8
- Miyoshi, Y., Shinohara, I., & Jun, C.-W. (2018c). The Level-3 orbit data of exploration of energization and radiation in geospace (ERG) Arase satellite [Dataset]. ERG. https://doi.org/10.34515/DATA.ERG-12001
- Miyoshi, Y., Shinohara, I., Takashima, T., Asamura, K., Higashio, N., Mitani, T., et al. (2018a). Geospace exploration project ERG. Earth Planets and Space, 70(1), 101. https://doi.org/10.1186/s40623-018-0862-0
- Morioka, A., & Miyoshi, Y. (2012). Two-step acceleration of auroral particles at substorm onset as derived from AKR spectra. In A. Keiling, E. Donovan, F. Bagenal, & T. Karlsson (Eds.), Auroral phenomenology and magnetospheric processes: Earth and other planets, Geophysical Monograph Series (Vol. 197, pp. 279–286). AGU. https://doi.org/10.1029/2011GM001160
- Morioka, A., Miyoshi, Y., Miyashita, Y., Kasaba, Y., Misawa, H., Tsuchiya, F., et al. (2010). Two-step evolution of auroral acceleration at substorm onset. *Journal of Geophysical Research*, 115(A11), A11213. https://doi.org/10.1029/2010ja015361
- Nishimura, Y., Lyons, L. R., Kikuchi, T., Angelopoulos, V., Donovan, E., Mende, S., et al. (2012). Formation of substorm Pi2: A coherent response to auroral streamers and currents. *Journal of Geophysical Research*, 117(A9), A09218. https://doi.org/10.1029/2012JA017889
- Olson, J. V. (1999). Pi2 pulsations and substorm onsets: A review. Journal of Geophysical Research, 104(A8), 17499–17520. https://doi.org/10.1029/1999ja900086
- Panov, E. V., Baumjohann, W., Nakamura, R., Kubyshkina, M. V., Glassmeier, K.-H., Angelopoulos, V., et al. (2014). Period and damping factor of Pi2 pulsations during oscillatory flow braking in the magnetotail. *Journal of Geophysical Research: Space Physics*, 119(6), 4512–4520. https://doi.org/10.1002/2013JA019633
- Panov, E. V., Nakamura, R., Baumjohann, W., Angelopoulos, V., Petrukovich, A. A., Retinò, A., et al. (2010). Multiple overshoot and rebound of a bursty bulk flow. Geophysical Research Letters, 37(8), L08103. https://doi.org/10.1029/2009GL041971
- Reeves, G. D., Fritz, T. A., Cayton, T. E., & Belian, R. D. (1990). Multi-satellite measurements of the substorm injection region. *Geophysical Research Letters*, 17(11), 2015–2018. https://doi.org/10.1029/GL017i011p02015
- Roux, A., Perraut, S., Robert, P., Morane, A., Pedersen, A., Korth, A., et al. (1991). Plasma sheet instability related to the westward traveling surge. Journal of Geophysical Research, 96(A10), 17697–17714. https://doi.org/10.1029/91JA01106
- Russell, C. T., Chi, P. J., Dearborn, D. J., Ge, Y. S., Kuo-Tiong, B., Means, J. D., et al. (2008). THEMIS ground-based magnetometers. *Space Science Reviews*, 141(1), 389–412. https://doi.org/10.1007/s11214-008-9337-0
- Saito, T., Yumoto, K., & Koyama, Y. (1976). Magnetic pulsation Pi2 as a sensitive indicator of magnetospheric substorm. *Planetary and Space*
- Science, 24(11), 1025–1029. https://doi.org/10.1016/0032-0633(76)90120-3
  Saka, O., Watanabe, O., Okada, K., & Baker, D. N. (1999). A slow mode wave as a possible source of Pi2 and associated particle precipitation:
- A case study. Annales Geophysicae, 17(5), 674–681. https://doi.org/10.1007/s00585-999-0674-4

  Sergeev, V. A., Bösinger, T., Belian, R. D., Reeves, G. D., & Cayton, T. E. (1992). Drifting holes in the energetic electron flux at geosynchronous orbit following substorm onset. Journal of Geophysical Research, 97(A5), 6541–6548. https://doi.org/10.1029/92JA00182
- Shiokawa, K., Katoh, Y., Hamaguchi, Y., Yamamoto, Y., Adachi, T., Ozaki, M., et al. (2017). Ground-based instruments of the PWING project to investigate dynamics of the inner magnetosphere at subauroral latitudes as a part of the ERG-ground coordinated observation network. *Earth Planets and Space*, 69(1), 160. https://doi.org/10.1186/s40623-017-0745-9
- Shiokawa, K., Yumoto, K., & Olson, J. V. (2002). Multiple auroral brightenings and associated Pi2 pulsations. Geophysical Research Letters, 29(11), 1537. https://doi.org/10.1029/2001GL014583
- Singer, H. J., Jr., Homes, E. W., & Rosenberg, T. J. (1988). Multipoint measurements from substorm onset to recovery: The relation between magnetic pulsations and plasmasheet thickening. *Advances in Space Research*, 8(9–10), 443–446. https://doi.org/10.1016/0273-1177(88)90158-5
- Solovyev, S. I., Baishev, D. G., Barkova, E. S., Molochushkin, N. E., & Yumoto, K. (2000). Pi2 magnetic pulsation as response on spatio-temporal oscillations of auroral arc current system. *Geophysical Research Letters*, 27(13), 1839–1842. https://doi.org/10.1029/2000gl000037
- Tian, S., Colpitts, C. A., Wygant, J. R., Cattell, C. A., Ferradas, C. P., Igl, A. B., et al. (2021). Evidence of Alfvenic Poynting flux as the primary driver of auroral motion during a geomagnetic substorm. *Journal of Geophysical Research: Space Physics*, 126(5), e2020JA029019. https://doi.org/10.1029/2020JA029019
- Tsyganenko, N. A., & Sitnov, M. I. (2005). Modeling the dynamics of the inner magnetosphere during strong geomagneticstorms. *Journal of Geophysical Research*, 110(A3), A03208. https://doi.org/10.1029/2004JA010798
- Turner, D. L., Fennell, J. F., Blake, J. B., Claudepierre, S. G., Clemmons, J. H., Jaynes, A. N., et al. (2017). Multipoint observations of energetic particle injections and substorm activity during a conjunction between Magnetospheric Multiscale (MMS) and Van Allen Probes. *Journal of Geophysical Research: Space Physics*, 122(11), 11481–11504. https://doi.org/10.1002/2017JA024554
- Uozumi, T., Yoshikawa, A., & Ohtani, S. (2020). Formation of a 3-D oscillatory current system associated with global high-correlation Pi 2 event: A case study. *Journal of Geophysical Research: Space Physics*, 125(1), e2019JA026988. https://doi.org/10.1029/2019JA026988
- Wang, S.-Y., Kazama, Y., Jun, C.-W., Chang, T.-F., Hori, T., Miyoshi, Y., & Shinohara, I. (2018a). The LEPe instrument level-2 omni-directional flux data of exploration of energization and radiation in geospace (ERG) Arase satellite [Dataset]. ERG. https://doi.org/10.34515/DATA. FRG-04002
- Wang, S.-Y., Kazama, Y., Jun, C.-W., Chang, T.-F., Hori, T., Miyoshi, Y., & Shinohara, I. (2018b). The LEPe instrument Level-2 3-D flux data of exploration of energization and radiation in geospace (ERG) Arase satellite [Dataset]. ERG. https://doi.org/10.34515/DATA.ERG-04001
- Yokota, S., Kasahara, S., Hori, T., Keika, K., Miyoshi, Y., & Shinohara, I. (2018a). The MEP-i instrument Level-2 omni-directional flux data of exploration of energization and radiation in geospace (ERG) Arase satellite [Dataset]. ERG. https://doi.org/10.34515/DATA.ERG-03001
- Yokota, S., Kasahara, S., Hori, T., Keika, K., Miyoshi, Y., & Shinohara, I. (2018b). The MEP-I instrument Level-2 3-D flux data of exploration of energization and radiation in geospace (ERG) Arase satellite [Dataset]. ERG. https://doi.org/10.34515/DATA.ERG-03000
- Yokota, S., Kasahara, S., Mitani, T., Asamura, K., Hirahara, M., Takashima, T., et al. (2017). Medium-energy particle experiments-ion mass analyzer (MEP-i) onboard ERG (Arase). Earth Planets and Space, 69(1), 172. https://doi.org/10.1186/s40623-017-0754-8

CHEN ET AL. 17 of 17